Theor. Appl. Climatol. 40, 9–23 (1989)

Theoretical and Applied Climatology

551.521

Department of Meteorology, University of Utah, Salt Lake City, Utah, U.S.A.

The Seasonal Cycle of the Global Zonally Averaged Energy Balance

Szu-cheng S. Ou, K. N. Liou and W. J. Liou

With 8 Figures

Received June 13, 1988
Revised July 28, 1988

Summary

The annual and seasonal cycle of the global zonally averaged storage and transport of moist static energy (MSE), the surface eddy flux of MSE, and the radiation budget at the top of the atmosphere (TOA) and surface are investigated in this paper. We use the GFDL (Geophysical Fluid Dynamics Laboratory) zonal mean data to compute the storage rate, divergence, and poleward flux of MSE. Surface eddy fluxes are determined based on an empirical formula developed from available climatological data. Radiative fluxes at the TOA and surface are computed from a radiation model. A number of significant features are illustrated by the present analysis in regard to the global annual and seasonal energy balance of the earth-atmosphere system. The storage/release rate of MSE is greater in spring and autumn than in summer and winter. The rate of poleward transport of MSE has a maximum at ~40 °N and ~35 °S with a value of $\sim 3 \times 10^{15}$ W. In terms of the radiation budget, the persistent ITCZ minimum and subtropical maxima of the IR flux distribution are reproduced well in the radiation parameterization program. The incoming solar flux maximum shifts from ~20 °N in spring to ~40 °N in summer due to the poleward increase in the fraction of daytime. Finally, an examination of the global surface energy balance reveals that the surface net fluxes derived from parameterizations for eddy and radiative fluxes agree well with values derived from observations. This agreement appears to imply that on the global mean, the physical parameterizations used in the present study are reliable in modeling the seasonal surface flux components.

Zusammenfassung

Der Jahresgang der zonal gemittelten globalen Energiebilanz

Der jährliche und jahreszeitliche Gang der globalen Zonenmittel der Speicherung und des Transports von latenter Energie (MSE), des Oberflächen-Eddy-Flusses der MSE und des Einstrahlungsbudgets an der Atmosphärengrenze (TOA) als auch auf der Erdoberfläche werden untersucht.

Wir verwenden die GFDL Zonenmitteldaten, um die Ladung, Divergenz und den polgerichteten Fluß der MSE zu errechnen. Die Oberflächen-Eddy-Flüsse werden aufgrund einer empirischen Formel bestimmt, die mittels verfügbarer klimatologischer Daten erstellt wurde. Strahlungsflüsse auf der Oberfläche und der Atmosphärengrenze werden mittels eines Einstrahlungsmodells errechnet. Eine Reihe signifikanter Erscheinungen werden in der vorliegenden Analyse dargestellt mit Hinblick auf das globale jährliche und jahreszeitliche Energiegleichgewicht des Erde-Atmosphäre-Systems. Die Ladungs- und Entladungsrate des MSE ist im Frühjahr und Herbst größer als im Sommer und Winter. Die Spitzen des polgerichteten Transports der MSE liegen bei 40° N und 35° S mit einem Wert von ca. 3×10^{15} W. In bezug auf das Einstrahlungsbudget werden die persistenten ITKZ-Minima und die subtropischen Maxima der IR-Flußverteilung gut von dem Einstrahlungsparameterisierungsprogramm dargestellt. Die Sonneneinstrahlungsflußspitzen verschieben sich von 20° N im Frühjahr nach 40° im Sommer aufgrund der gegen den Pol hin zunehmenden Tageslänge. Zuletzt zeigen die Untersuchungen des globalen Oberflächenenergiegleichgewichts auf, daß die Oberflächennettoflüsse, abgeleitet von der Parameterisierung für Eddy- und Einstrahlungsflüsse, mit den beobachteten Werten gut übereinstimmen. Diese Übereinstimmung impliziert offensichtlich, daß im globalen Durchschnitt die physikalische Parametrisierung, die in dieser Studie angewendet wurde, verläßliche Modelle der jahreszeitlichen Oberflächenflußkomponenten liefern kann.

1. Introduction

All energy balance climate models are based on the conservation of the dynamic transport of moist

static energy (MSE) and absorption/emission of radiative energy. Thus, the verification of climate models must include comparisons of the model-produced MSE transport and radiative flux fields with those analyzed from climatological data. Several sets of global-scale climatological statistics for dynamic and radiative flux fields are available for verification of climate models. Based on surface reports from May 1958 through April 1963, Oort and Rasmusson (1971) generated extensive atmospheric general circulation statistics for the Northern Hemisphere. Oort (1983) further expanded these statistics to include the Southern Hemisphere, and extended the period of data analysis from 1958 to 1973 (referred to here as the GFDL data tape). These statistics include the zonal and meridional wind fields, geopotential height, temperature, humidity, and flux fields for the transport of sensible and latent heat. In addition, Oort and Péixoto (1983) presented the storage rate and divergence of the transport of MSE for summer, winter, and annual averages based on the GFDL data tape.

Radiances measured by satellites have been used to produce a seasonal/monthly radiation budget. Vonder Haar and Suomi (1971) presented a global map of net radiative fluxes at the top of the atmosphere (TOA) based on observed radiance data during the period 1962–1966. Oort and Vonder Haar (1976) presented the budget of solar and infrared fluxes at the TOA based on radiances measured from polar orbiting satellites. More recently, Stephens et al. (1981) updated the zonally averaged radiation budget for the period 1964–1977, and included calculations of surface radiation budgets using a radiative transfer model.

The objectives of the present study are to present statistics for the annual and seasonal cycle of MSE transport, and to test the applicability of the radiative transfer and surface turbulent flux parameterizations that were developed in our previous studies (Liou and Ou, 1983; Ou and Liou, 1984). Three aspects of thermodynamic energy conservation are investigated. These include: 1) the vertically integrated storage and poleward transport of MSE, 2) the radiation balance at the TOA and surface, and 3) the surface thermodynamic energy balance. In this study, we have carried out computations of the storage rate and divergence of poleward transport of MSE for all seasons. In addition, radiation budgets are calculated using the radiation parameterization scheme developed by Liou and Ou (1983), based on the mean seasonal climatology of cloud parameters, surface albedo, solar zenith angle, temperature and humidity. Radiative fluxes at the TOA are verified using the observed data presented by Stephens et al. (1981). The global earth-atmosphere energy balance is subsequently examined. The energy balance components are divided into two groups, including quantities derived from observations and model calculations. The residuals of these two components are the surface net fluxes. This division allows us to check the reliability of the results derived from model calculations.

In Section 2, the balance relationship for the transport of MSE, the principles of modeling solar and infrared radiative exchanges, and a simple surface turbulent flux parameterization are briefly described. In Section 3, the storage rate and flux fields analyzed for MSE, along with the surface turbulent flux distribution obtained from parameterizations are presented. The computed global radiation budget is compared with satellite-derived results and the global surface energy balance is then examined. Finally, conclusions are given in Section 4.

2. Theoretical Background

2.1 Dynamic Energy Transport

The moist static energy may be expressed in the form

$$E = C_p T + gz + Lq \,, \tag{2.1}$$

where C_p is the specific heat for air at constant pressure, T the temperature, g the gravitational accelerlation, z the height, L the latent heat per unit mass, and q the water vapor mixing ratio. Based on the first law of thermodynamics, conservation of the thermodynamic energy may be written

$$\frac{\mathrm{d}}{\mathrm{d}t}(\rho E) = \frac{\partial}{\partial t}(\rho E) + \nabla \cdot \boldsymbol{v} E = -\nabla \cdot \boldsymbol{F} \,, \tag{2.2}$$

where ρ is the air density, $\boldsymbol{v}$ the velocity vector, and $\boldsymbol{F}$ the three-dimensional radiative flux density. We then carry out temporal and zonal averages. The variables E, $\boldsymbol{F}$, and $\boldsymbol{v}$ are first separated into a time mean and a deviation term, which are symbolized by an overbar and a prime, respectively.

After carrying out the time averaging procedure, Eq. (2.2) becomes

$$\frac{\Delta}{\Delta t}\bar{\rho}\bar{E} + \nabla\cdot\rho\,\bar{v}\bar{E} + \nabla\cdot\rho\,\overline{v'E'} = -\nabla\cdot\bar{F}\,, \qquad (2.3)$$

where the first term on the left-hand side is the averaged storage rate of MSE within the time period Δt, and the second and third terms denote the divergence of mean and transient eddy fluxes of MSE, respectively.

In a manner similar to the time averaging procedure, arbitrary variables may also be separated into a zonal mean and a deviation, which are symbolized by a pair of brackets and an asterisk, respectively. After carrying out zonal averaging, the zonal mean balance quation may be derived from Eq. (2.3) in the form

$$\frac{\Delta}{\Delta t}[\bar{\rho}][\bar{E}] = \frac{-1}{a\cos\varphi}\frac{\partial(F_h\cos\varphi)}{\partial\varphi} - \frac{\partial F_v}{\partial z} - \frac{\partial}{\partial z}[\bar{F}]\,, \qquad (2.4)$$

where

$$F_h = [\bar{\rho}]([\bar{v}][\bar{E}] + [\bar{v}^*\bar{E}^*] + [\overline{v'E'}])\,, \qquad (2.5)$$

$$F_v = [\bar{\rho}]([\bar{w}][\bar{E}] + [\bar{w}^*\bar{E}^*] + [\overline{w'E'}])\,, \qquad (2.6)$$

and λ is the latitude, a the mean earth radius, and $[\bar{F}]$ the temporally and zonally-averaged radiative flux, which varies only in the vertical direction. In Eq. (2.4), the left-hand side denotes the zonally averaged rate of storage, while the first, second, and third terms on the right-hand side represent the horiztontal, vertical, and radiative flux divergences, respectively. Equations (2.5) and (2.6) define the total poleward and vertical fluxes. The first, second, and third terms on the right-hand side of these two equations denote the mean, stationary, and transient eddy fluxes of MSE, respectively.

We then perform an integration in the z-direction from the surface to the TOA using Eq. (2.4), and obtain a column energy balance equation:

$$S_A = -F_H + F_v(0) + F_N(0) - F_N(z_t)\,, \qquad (2.7)$$

where

$$S_A = \frac{1}{\Delta t}\int_0^{z_t}\Delta([\bar{\rho}][\bar{E}])\,\mathrm{d}z\,, \qquad (2.8)$$

$$F_H = \frac{1}{a\cos\varphi}\frac{\partial}{\partial\varphi}\int_0^{z_t}F_h\cos\varphi\,\mathrm{d}z\,, \qquad (2.9)$$

and $F_v(0)$, $F_N(0)$, and $F_N(z_t)$ represent, respectively, the surface turbulent flux and the net upward radiative fluxes at the surface and TOA. The quantities S_A and F_H are the vertically integrated mean storage rate and divergence of the poleward flux of MSE, respectively. Equation (2.7) is the basic energy balance equation for an atmospheric column in which the total heat storage rate is balanced by the surface input $[F_v(0) + F_N(0)]$ minus the sum of the divergence of poleward transport fluxes and the net radiative flux at the TOA. Finally, the poleward transport rate of MSE, $P_f(\varphi)$, is defined as

$$P_f(\varphi) = 2\pi a\int_0^{z_t}F_h(\varphi)\,\mathrm{d}z\,. \qquad (2.10)$$

2.2 Radiative Transfer Parameterizations

The radiative transfer parameterizations followed the program developed by Liou and Ou (1983) and Ou and Liou (1984). For infrared radiative transfer, we employ a broadband flux emissivity approach. We divide the entire infrared spectrum into five bands: three for water vapor, one for CO_2, and one for O_3 absorption. The flux emissivity is expressed in terms of a polynomial function of the corrected path length for water vapor and ozone based on band-by-band calculations. For the CO_2 15 μm band, the flux emissivity is parameterized based on the transmittance values derived from line-by-line integrations according to Ou and Liou (1983). For cloudy atmospheres, we assume that there are six cloud types and neglect the overlap effect. The broadband infrared emissivity, reflectivity, and transmissivity for cirrus clouds are prescribed as functions of the vertical ice/liquid water path, following the parameterization equation developed by Liou and Wittman (1979). All other cloud types are treated as blackbodies.

For solar radiative transfer, the spectrum is divided into 25 bands: 6 for H_2O, 1 for CO_2, which overlaps the H_2O 2.7 μm band, and 18 for O_3. The absorptivities for the H_2O and CO_2 bands are calculated according to Liou and Sasamori (1975). For ozone, the absorptivity is computed based on the absorption coefficient values compiled by Howard et al. (1961). The determination of clear-sky fluxes is based on known values of the solar zenith angle and absorptivity. For the cloudy case,

the broadband solar reflection and transmission values for various cloud types are obtained from polynominal functions of the cloud liquid water path and solar zenith angle (Liou and Wittman, 1979). The net solar fluxes above and below the cloud are then determined based on the functional values of gaseous absorptivities, cloud optical properties, and the generation function, which is introduced to account for the effects of cloud-cloud and cloud-surface multiple reflections.

2.3 Surface Vertical Transport

As illustrated in Eq. (2.6), the vertical transporet of MSE consists of a mean tranport, and transient and stationary eddy fluxes. The stationary eddy flux is very small and can be neglected (Oort and Rasmusson, 1971). The mean MSE flux depends on the vertical velocity, temperature, geopotential height, and humidity. Only the transient eddy term needs to be parameterized. In theory, the modeling of the surface transient eddy flux should be based on boundary layer physics, taking into account soil moisture, vegetation, ground water, ocean roughness, etc. However, the parameterization of large-scale surface eddy fluxes for use in climate modeling must be computationally efficient. We used an empirical relationship for the surface eddy flux proposed by Ou and Liou (1984) in the form

$$\rho[\overline{w'E'}]_{z\to 0} = c_1\left[\left|\frac{\partial T}{\partial z}\right| + \frac{L}{C_p}\left|\frac{\partial q}{\partial z}\right|\right]^{c_2}_{z\to 0}. \tag{2.11}$$

Statistical analyses were carried out to determine the coefficients c_1 and c_2. In these analyses, we used the surface flux data estimated by Sellers (1965) and Budyko (1982), along with the temperature and humidity data from Oort (1983). The temperature gradient $\partial T/\partial z$ is evaluated at 975 mb. The humidity gradient $\partial q/\partial z$ is computed from the difference between the water vapor mixing ratio at (1000-ΔP) mb, and its saturated value at 1000 mb. Three different values of ΔP (5, 10, and 15 mb) were selected to determine the two gradient terms. A linear regression analysis was then performed to determine c_1, c_2, and the correlation coefficient. It was found that $\Delta P = 15$ mb gives the highest correlation coefficient with $c_1 = 12.02$ and $c_2 = 0.53$, respectively.

3. Results and Discussion

3.1 Data Sources

A portion of the GFDL Tape Library, which contains the zonal mean data, was used for the analysis of large-scale poleward transport of MSE by mean motions and eddies. The 1963–1973 period was selected for this study rather than the entire 15-year period because the Southern Hemishere data were not available in the first five years. For radiation computations, the mean length of the day and the cosine of the solar zenith angle for all seasons wwere taken from Manabe and Möller (1961). The total cloud cover and average amount and height for six cloud types over the Northern Hemisphere were taken from London (1957). The cloud cover over the Southern Hemisphere was taken from Sasamori et al. (1972). Since Sasamori et al. (1972) did not provide values for the total cloud cover, fractional covers for all types of clouds were added. This may result in a slight overestimation of the total cloud cover. The cloud thicknesses for various types of cloud were based on the values given in Liou et al. (1984), and the surface albedos were taken from the values listed in Robock (1980). Finally, the ozone densities for various pressure levels and seasons were based on profiles presented by McClatchey et al. (1971).

3.2 Atmospheric Poleward Transport Statistics

The zonally averaged global data that were used consisted of a group of 20×85 array of monthly, seasonal, and annual mean values for various parameters. The vertical and meridional resolutions are 50 mb and 2° latitude, respectively. Each year was divided into four seasons, and each season (Δt) consisted of about 121.5 days. The surface value of each variable was assumed to be the same as the 1000 mb value, except in the subantarctic area where the surface value is obtained by extrapolation, since the surface pressure there is less than 1000 mb.

To obtain the MSE storage rate, S_A, based on Eq. (2.8) for each latitudinal grid point, the mean MSE was first calculated for all seasons at each pressure level, and then integrated vertically using the trapezoidal rule. The central differencing scheme was employed to compute the rate of MSE storage for each season. Figure 1 shows the latitudinal distribution of S_A for each season. The

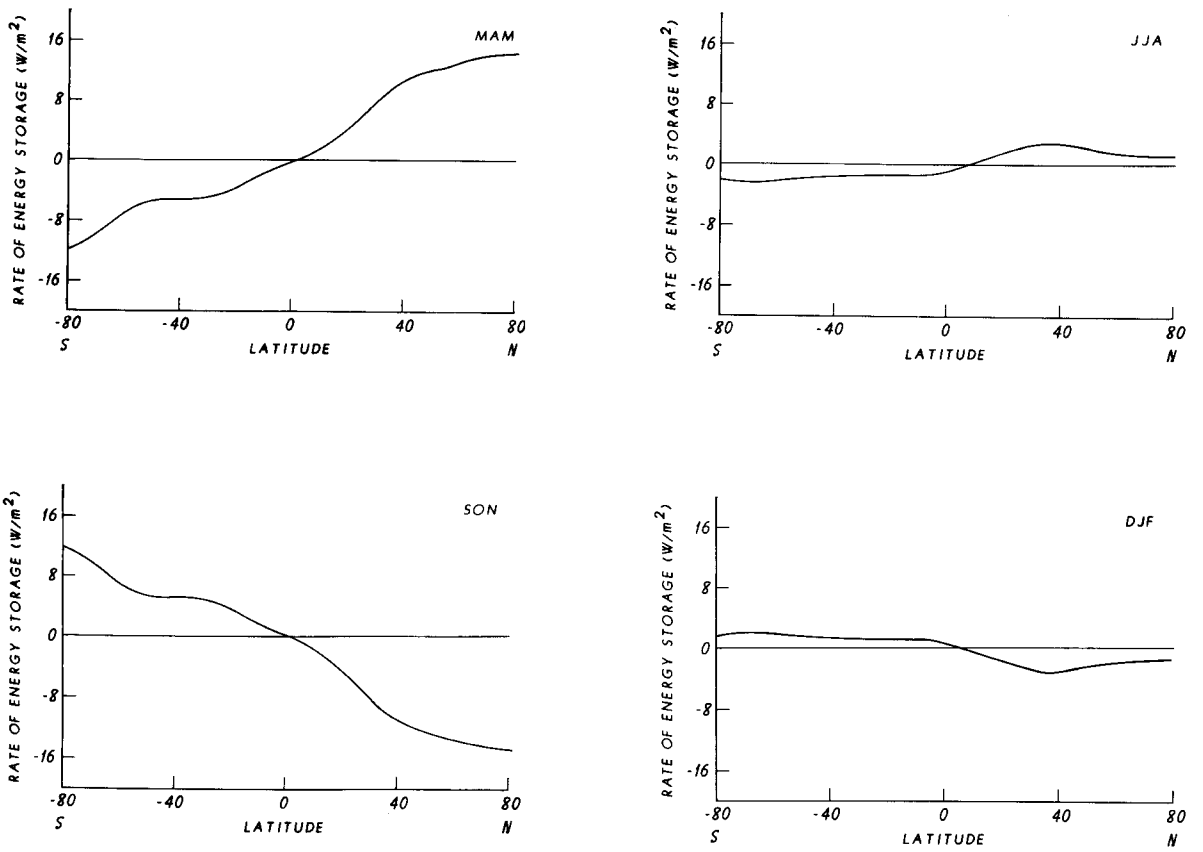

Fig. 1. Latitudinal distribution of the rate of energy storage in the atmosphere

annual mean storage rate should be zero and is not shown. As noted in Fig. 1, because of the small heat capacity of air, values for S_A are relatively small. For the seasons DJF (December, January, and February) and JJA (June, July, and August) the storage/release rate in both hemispheres is less than $4\,W/m^2$, whereas in the transition seasons, MAM (March, April, and May) and SON (September, October, and November), a large storage/release rate ($12 \sim 16\,W/m^2$) occurs at higher latitudes due to the large temperature change between summer and winter. The maximum heat storage/release occurs in the predominantly continental subarctic regions, because the seasonal rate of fluctuation of temperature is larger over land., The present curves for JJA and DJF are identical to those given by Oort and Péixoto (1983). We also note that there is relatively little MSE storage/release in the tropical region for all seasons, due to small variations in the solar zenith angle.

To obtain the divergence of the poleward transport of MSE, F_H, the poleward transport fluxes, F_h, were computed based on Eq. (2.5) at each latitudinal grid point and pressure level, and then integrated vertically using the trapezoidal rule. Subsequently, the latitudinal derivatives were obtained by central-differencing using Eq. (2.9). The annual and seasonal latitudinal distribution of F_H is shown in Fig. 2, along with the results for JJA, DJF, and the annual average presented by Oort and Péixoto (1983). The present results have been smoothed using a 5-point average scheme and are slightly different from those of Oort and Péixoto (1983), probably due to the smaller finite-differencing intervals used in the present computations. However, the two sets of computations basically agree with each other, both in magnitude and sign. A zone of significant positive divergence (~ 30–$40\,W/m^2$) is present in the subtropics of the summer hemisphere, while in the polar region of the winter hemisphere large negative divergence (convergence, ~ 60–$130\,W/m^2$) exists. A positive (negative) divergence implies a net heat loss (gain). In general, the seasonal variation of the transport

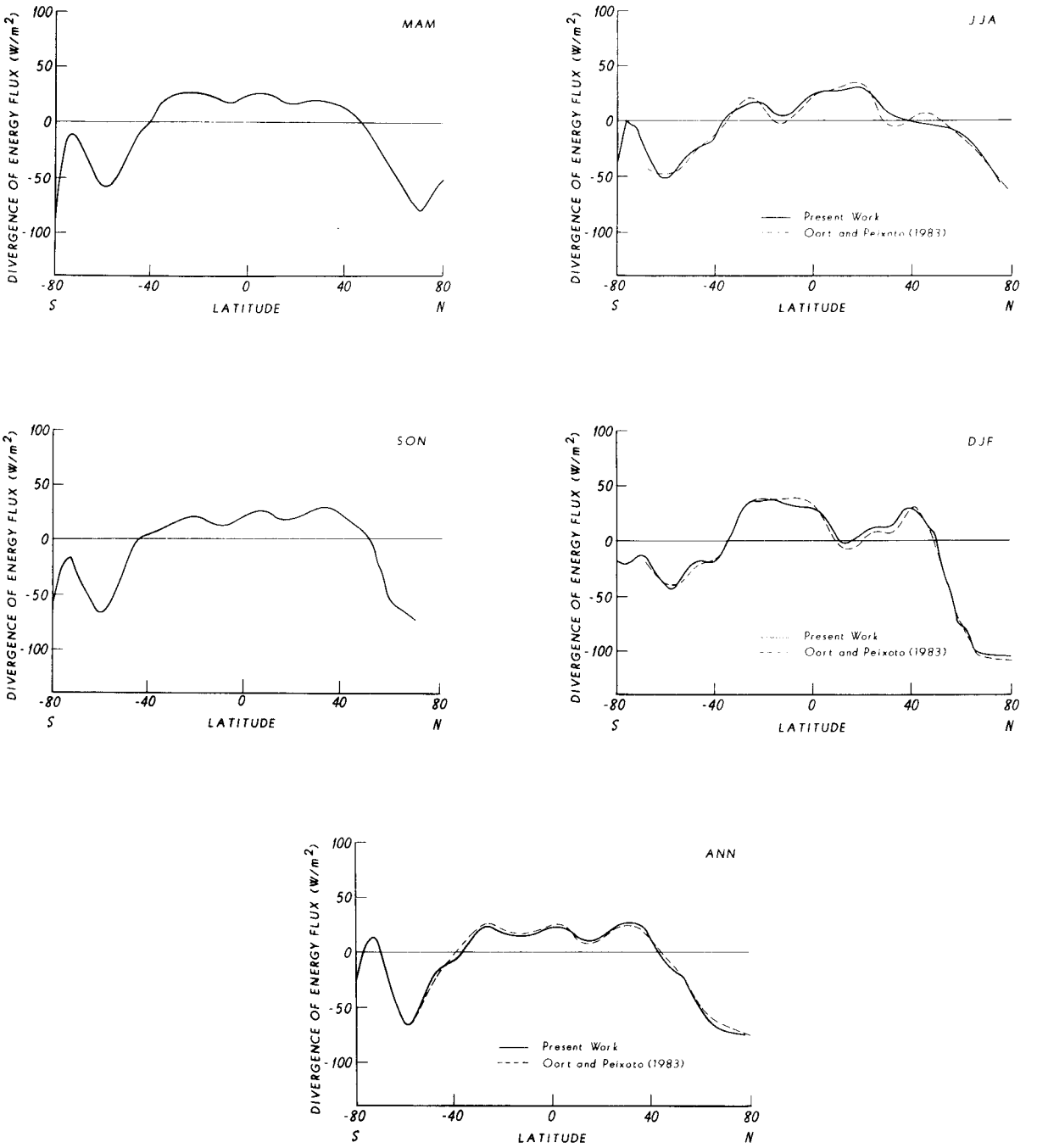

Fig. 2. Latitudinal distribution of the divergence of the vertically integrated atmospheric transport of energy

divergence in the Southern Hemisphere is relatively small when compared with that in the Northeren Hemisphere due to the presence of primarily oceans there.

The rate of poleward transport of MSE was obtained numerically according to Eq. (2.10). Figure 3 shows the annual and seasonal latitudinal distribution of the rate of MSE poleward transport, where positive (negative) values imply northward (southward) transports. Oort and Péixoto (1983) did not present the seasonal variation in this quantity. However, in an earlier paper, Oort and Vonder Haar (1976) presented the annual mean rate of poleward transport of MSE for the Northern Hemisphere using the data for the period 1958–1963. The present values, analyzed from

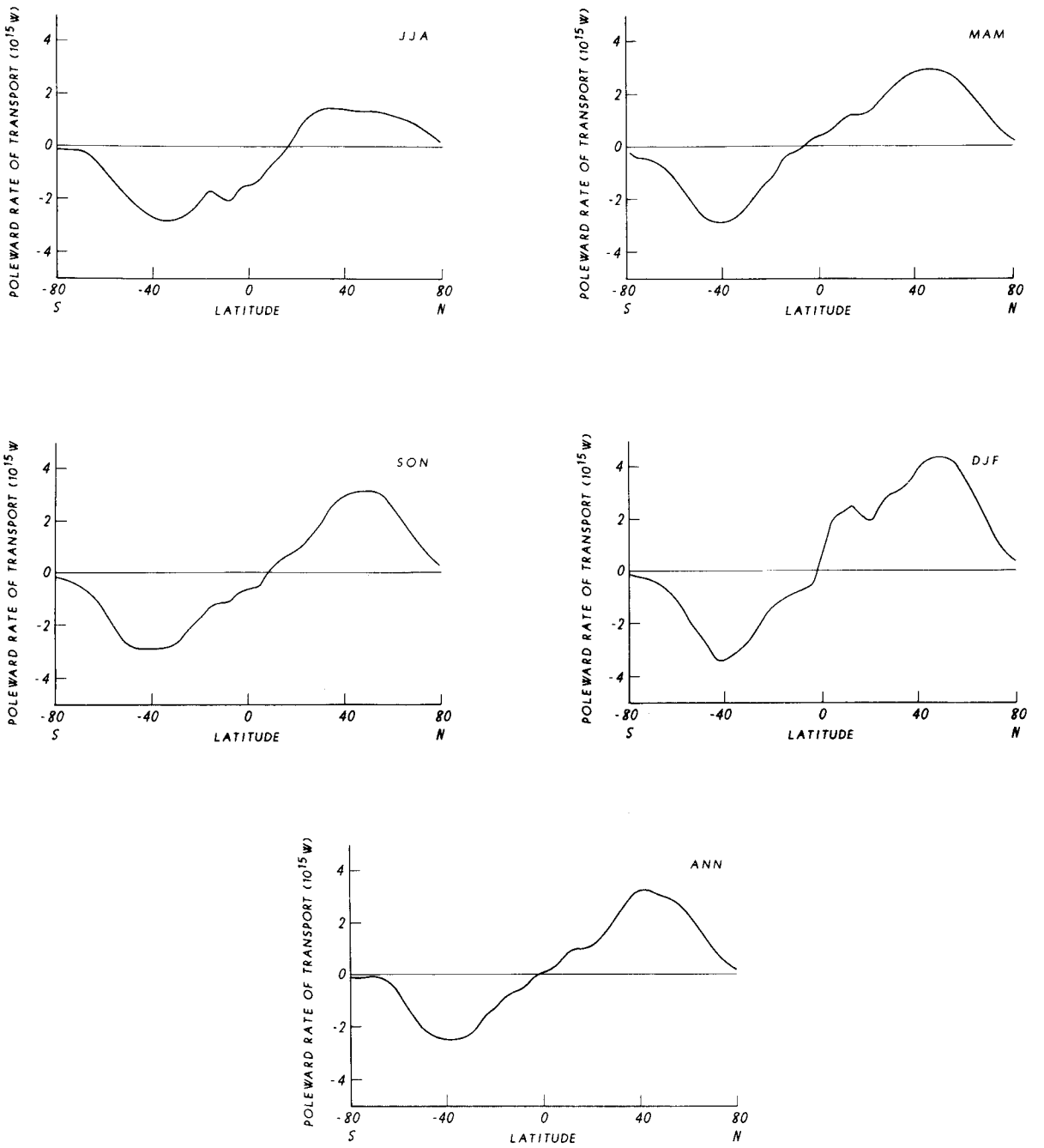

Fig. 3. Latitutinal distribution of the northward transport of energy in the atmosphere

the 1963–1973 data, agree with their results. The maximum transport rate is larger ($\sim 4.5 \times 10^{15}$ W) in the winter than in the summer ($\sim 2 \times 10^{15}$ W) for the Northern Hemisphere due to larger values of F_H. For the Southern Hemisphere, no significant seasonal variation in the transport pattern is seen. Annually, the maximum transport rate is about 3×10^{15} W for both hemispheres, and occurs at $\sim 40\,^{\circ}$N and $\sim 35\,^{\circ}$S. The transport of MSE from the summer hemisphere to the winter hemisphere, due to the migration of the ITCZ, is also evident in this figure.

For the surface eddy flux, Fig. 4 shows a comparison between the results computed by the parameterization described in Section 2 and the annual values estimated by Budyko (1982) and Sel-

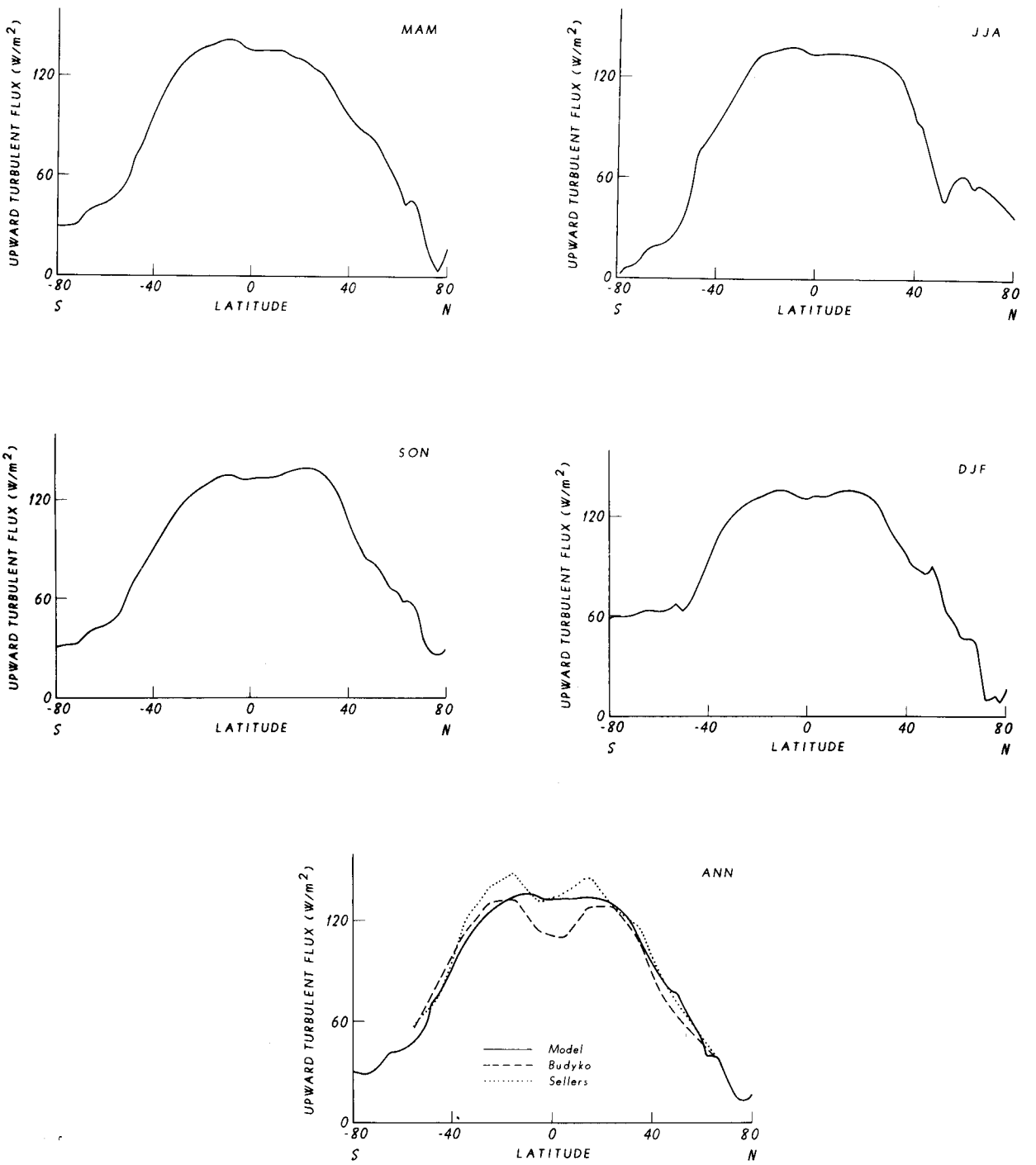

Fig. 4. Latitudinal distribution of the surface upward turbulent flux. The data from Budyko (1982) and Sellers (1965) are also depicted in the diagram

lers (1965). Good agreements between calculations and climatological data are evident in the extratropical area. However, the contrast between the subtropical maximum and equatorial minimum is not as sharp as the climatology. It is noted that the zonally-averaged temperature and humidity gradients near the surface used in the calculations are largely based on observations over land. However, the actual gradients in the subtropical regions are higher due to ocean current effects (Sellers, 1965), whereas they are lower in the tropics due to lower ocean temperatures. Using the same par-

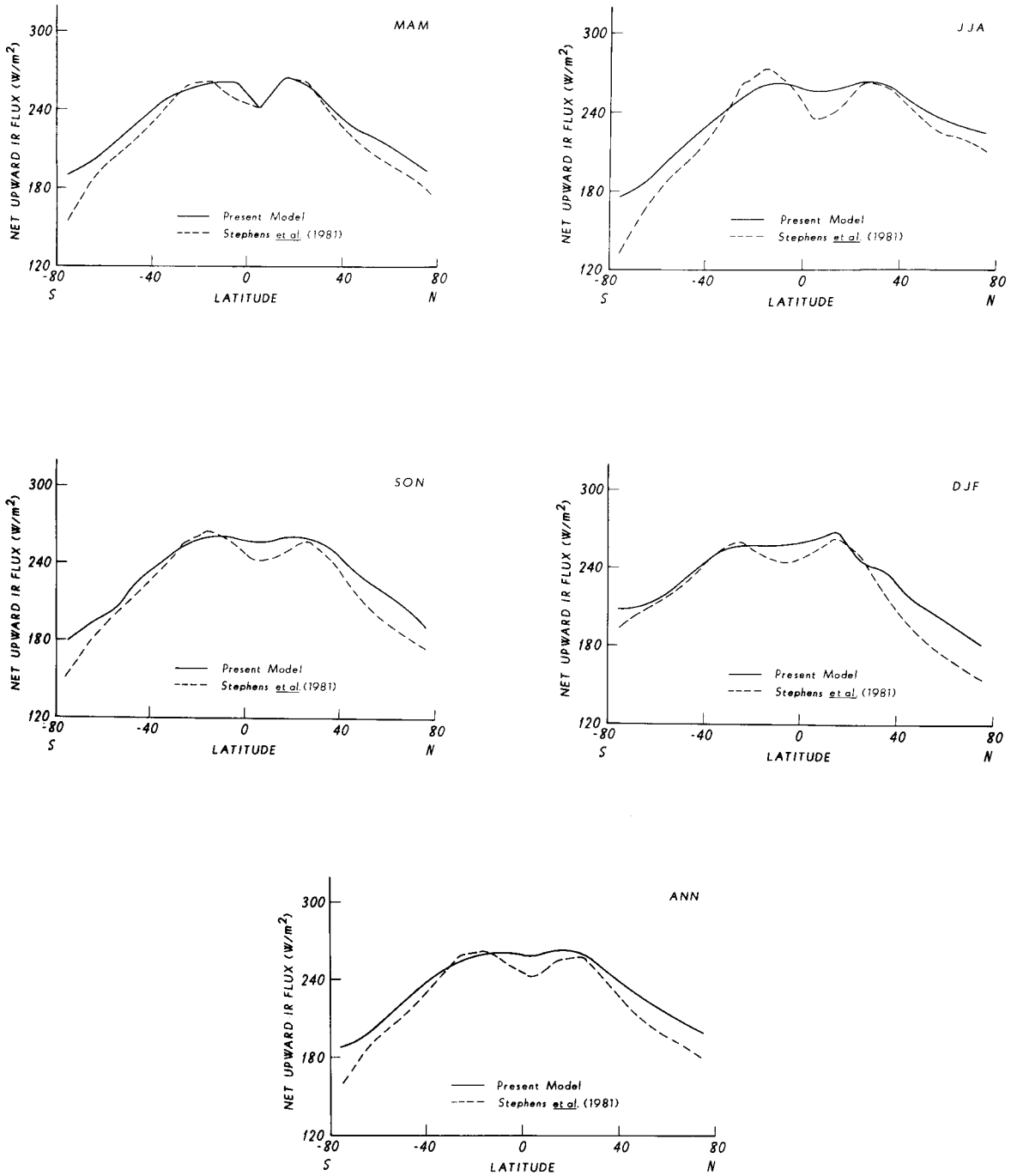

Fig. 5. Latitudinal distribution of the net upward IR flux at the top of the atmosphere. Data from Stephens et al. (1981) are also presented for comparison

ameterization, seasonal values for the surface eddy fluxes are displayed in Fig. 4. The seasonal results differ insignificantly from the annual case, except at higher latitudes in the summer hemisphere, where significant increases in the surface temperature and humidity gradients occur.

3.3 Radiation Budget

In this section we present the computed global seasonal and annual radiation budgets based on the input data described in Section 3.1. Figure 5 shows the latitudinal distribution of the outgoing

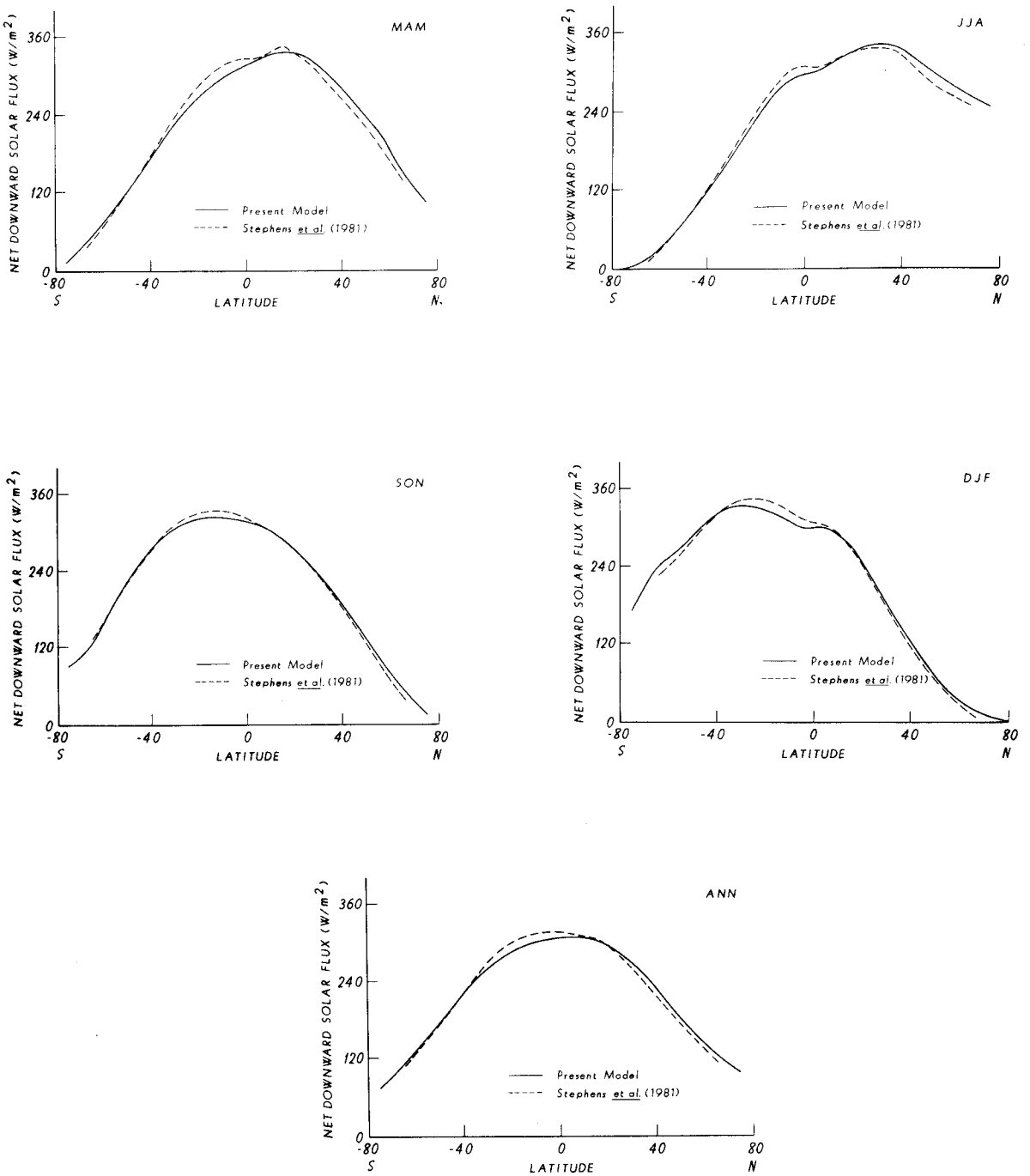

Fig. 6. Latitudinal distribution of the net downward solar flux at the top of the atmosphere. Data from Stephens et al. (1981) are also shown for comparison

infrared flux at the TOA. The current model resuls are systematically higher than the values presented by Stephens et al. (1981) in the extratropics. The differences may be caused by uncertainties in the model prescription of the cloud cover distribution. Because of the smaller cloud cover in the area of subtropical highs, there are maxima of infrared fluxes at ~20 °N and ~25 °S for all seasons. A slight dip over the ITCZ indicates the effects of extensive cloudiness and high humidity content. The contrast between the subtropical maximum and the equatorial minimum is less for the present

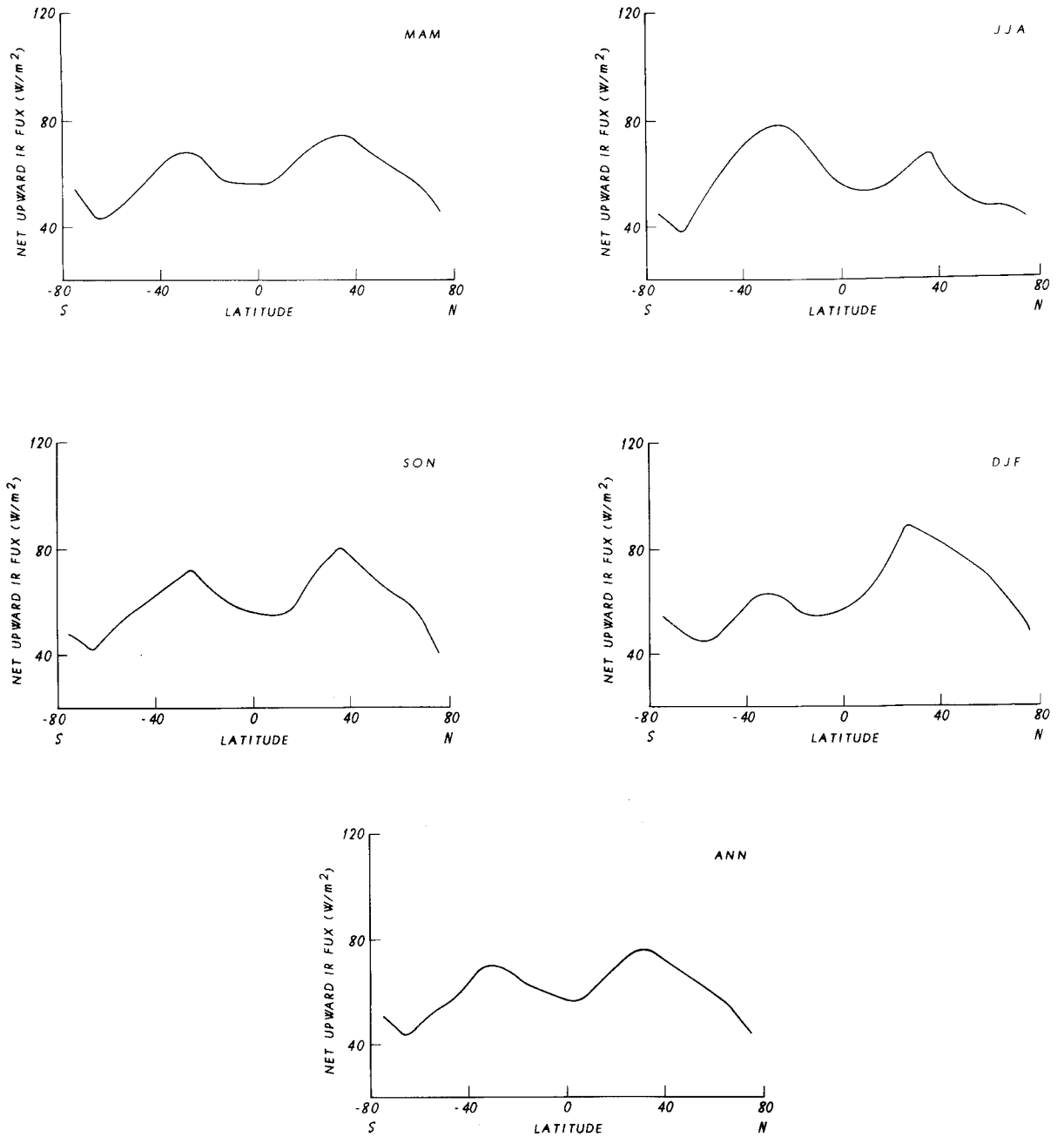

Fig. 7. Latitudinal distribution of the net upward IR flux at the earth's surface

model, possibly due to an uncertainty in the prescribed tropical cirrus cloud height and emissivity. Lower infrared flux values are found at high latitudes, especially in the winter hemisphere, due to lower temperatures. Seasonal variations are more pronounced in the polar regions in both summer and winter.

The meridional profile of the solar flux at the TOA is shown in Fig. 6. Annually, the solar flux pattern has a maximum of $\sim 320\,W/m^2$ near the equator and decreases poleward. On a seasonal basis, the maximum solar flux occurs near 20° in the spring and near 40° in the summer. This is because additional solar flux is absorbed by the atmosphere due to a larger fraction of daytime near the summer polar region. The observed solar flux, derived from the monthly zonal mean planetary albedo tabulated by Stephens et al. (1981),

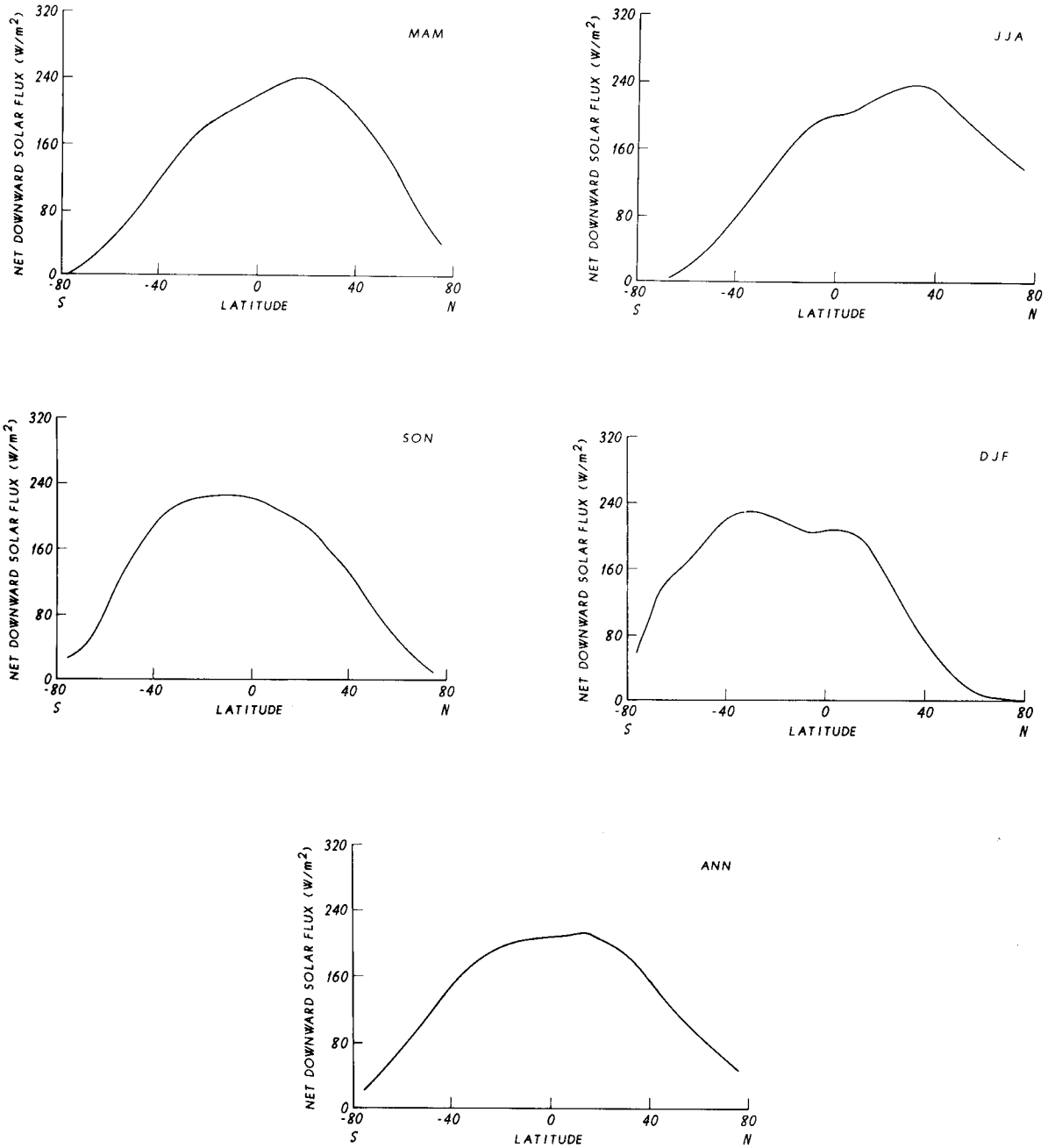

Fig. 8. Latitudinal distribution of the net downward solar flux at the earth's surface

is also plotted in Fig. 6 for comparison purposes. The observations and model computations are in general agreement, except for a small difference in the Southern Hemisphere between the equator and 40 °S. This discrepancy might be due to an uncertainty in the total cloud cover distribution. The derived global mean albedo is 31%, which is the same as the value obtained from satellite measurements.

Figure 7 shows the zonal mean emitted infrared flux at the surface. The net emission is larger in the winter than in the summer, mainly because the atmosphere is drier in winter. There are two peaks at ~30 °N and ~30 °S, which correspond to the locations of subtropical highs. Similar to the infrared flux distribution at the TOA, a dip over the ITCZ is also present. The computed results for the annual case agree well with other

calculations (Stephens et al., 1981). The surface infrared fluxes are between ~40 and 100 W/m^2, but are not verifiable due to a lack of observations.

The latitudinal distributions of the surface net solar flux are shown in Fig. 8. The pattern is similar to the solar flux at the TOA shown in Fig. 6. This implies that the absorption of solar radiation in the atmosphere is nearly independent of latitude. The maxima in the spring and summer are about 200 and 240 W/m^2 at 20° and 40° latitudes, respectively. Annually, the Northern Hemisphere receives slightly more solar radiation at the surface than the Southern Hemisphere, probably due to the lower total cloudiness.

3.4 An Overview of the Global Surface Energy Balance

We have examined various components of the atmospheric energy balance. In this section, we shall investigate the requirements of the atmospheric and surface energy balance relationships by combining these components. Based on Eq. (2.7), the energy components may be divided into two groups: 1) quantities that can be derived from observations, including F_H, S_A, and $F_N(z_t)$, and 2) quantities for which global-scale observations are not yet available, including $F_N(0)$ and $F_v(0)$. Eq. (2.7) may be rewritten as follows:

$$F_H + S_A + F_N(z_t) = F_N(0) + F_v(0) , \qquad (3.1)$$

where all the terms on the left-hand side of Eq. (3.1) may be derived from available measurements, while the terms on the right-hand-side may be theoretically computed. Based on the surface energy balance, the right-hand side also represents the net energy flux exchange between the surface and atmosphere. Thus, we may define the downward surface net flux, computed from parameterization programs, in the form

$$R_1 = -[F_N(0) + F_v(0)] . \qquad (3.2)$$

The surface net flux evaluated from observations is then given by

$$R_2 = -[F_H + S_A + F_N(z_t)] . \qquad (3.3)$$

A comparison of R_1 and R_2 illustrates the reliability of the radiative transfer and surface turbulent flux parameterizations. $F_N(0)$ and $F_v(0)$ in Eq. (3.2) were computed from the radiative transfer and surface turbulent flux parameterizations described in subsections 2.2 and 2.3, respectively. The quantities F_H and S_A in Eq. (3.3) were determined from general circulation statistics (Oort, 1983). The seasonal and latitudinal distributions of these quantities were presented in subsection 3.3. Finally, the quantity $F_N(z_t)$ was taken from the zonally averaged latitudinal distribution of net radiative fluxes at the TOA derived from satellite radiance measurements (Stephens et al., 1981). Table 1 lists the global mean values for F_H, S_A, $F_N(z_t)$, R_1, $F_N(0)$, $F_v(0)$, R_2, and R_1–R_2 for four seasons and the annual mean. The global mean values were obtained by integration of the latitudinal values from 75 °S to 75 °N. Seasonal values of F_H are no greater than 2 W/m^2. This indicates that the general circulation data satisfy the physical requirement that, on a global scale, there should be no net divergence due to horizontal transport. The net radiative flux at the TOA shows that there is a constant heat input in all seasons for the period 1964–1967. Stephens et al. (1981) stated that this global net radiative input is probably due to the differences in hemispheric cloudiness and land-ocean distribution. The net radiative input also varies with season due to variations in the earth-sun distance. In DJF the net input reaches 15 W/m^2 when the earth is closest to the sun, while in JJA its magnitude is only 1 W/m^2. The effect of the net radiative input is reflected in R_2, which is positive (except in JJA), implying that most of the net radiative input is stored in the earth itself, presumably the ocean. The parameterized values $F_N(0)$ range between 92 to 101 W/m^2. The present annual value of 98 W/m^2 is between the estimates of 95 W/m^2 and 102 W/m^2 derived by Sellers (1965) and Budyko (1982), respectively. The surface eddy flux parameterization yields a range of $F_v(0)$ between 100 and 103 W/m^2, which compares well with estimates of the annual mean by Sellers (1965) and Budyko (1982). The resulting values of R_1 from parameterizations vary between 0 and −10 W/m^2. R_1 differs from R_2 by 1 W/m^2 in JJA and −25 W/m^2 in DJF. These differences are on the same order as the uncertainty in surface radiation budgets derived from satellite radiance observations. Based on 29 months of observed data, Oort and Vonder Haar (1976) reported that the uncertainty in the annual cycle of the surface net flux fields is ~10 to 20 W/m^2.

Table 1. *The Global Mean of the Energy Balance Components* (in units of W/m^2)

	F_H	S_A	$F_N(z_T)$	R_2	$F_N(0)$	$F_v(0)$	R_1	R_1-R_2
MAM	1	2	− 9	6	−101	103	− 2	− 8
JJA	2	0	− 1	−1	−100	100	− 0	1
SON	1	−2	−11	12	− 98	103	− 5	−17
DJF	0	0	−15	15	− 92	102	−10	−25
Annual	1	0	−10	9	− 98	102	− 4	−13

4. Conclusions

In this paper we investigated the annual and seasonal cycles of the global zonally averaged storage and transport of MSE, the surface eddy flux of MSE, and radiative energy exchange. The GFDL zonal mean data were used to derive the storage rate and divergence, and the poleward flux of MSE. The radiation budgets at the surface and TOA were computed based on a radiation parameterization model, while the surface eddy fluxes were determined from an empirical parameterization.

Several significant features were shown in regard to the global seasonal and annual energy balance of the earth-atmosphere system. The storage/release rate of MSE is less than $4\,W/m^2$ for DJF and JJA, but increases to $12–16\,W/m^2$ at higher latitudes in the transition seasons of MAM and SON due to the large temperature change between summer and winter. For the poleward transport of MSE, a zone of significant positive divergence ($\sim 30–40\,W/m^2$) is present in the subtropics during the summer season, while the polar regions show a large negative divergence in the winter season. In terms of the rate of the poleward transport of MSE, the maximum value is about 3×10^{15} W and occurs at 40 °N and 35 °S. The mean surface transient eddy fluxes computed from the present model vary insignificantly between seasons. In terms of the radiation budget at the TOA, the infrared and solar fluxes computed from the model agree reasonably well with satellite data presented by Stephens et al. (1981). The IR flux distribution shows maxima at ~20 °N and 25 °S for all seasons, as well as a persistent minimum in the TICZ region. These features are noticeable in the radiation model. For the solar flux distribution, the maximum occurs near ~20° in the spring and near ~40° in the summer. The seasonal variation in the latitude of maximum solar input is due to a longer daytime in the summer. The net infrared and solar flux distributions at the surface show trends similar to those at the TOA.

Finally, an examination of the global surface energy balance reveals that the surface net flux can be derived either by observations or theoretical calculations. The former contains the observed data for the radiation budget at the TOA and the storage and transport of MSE. The latter involves calculations of the surface radiative and eddy fluxes by using parameterizations. A comparison of these two surface net fluxes shows that they basically agree with each other. On a global mean basis, the physical parameterizations presented in this paper appear to be reliable for modeling the seasonal distribution of surface radiative and eddy fluxes.

Acknowledgements

The research was supported by NASA Grant NAG5-732 and in part by the Air Force Office of Scientific Research Grant AFOSR-87-0294. The authors are grateful to Dr. A. H. Oort for his helpful comments on the paper.

References

Budyko, M. I., 1982: *The Earth's Climate: Past and Future.* New York: Academic Press, 307 pp.

Howard, J. N., King, J. I. F., Gast, P. R., 1961: Thermal radiation. In: *Handbook of Geophysics*, New York: MacMillan, Chapter 16. 964 pp.

Liou, K. N., Ou, S. S., 1983: Theory of equilibrium temperature in radiative turbulent atmospheres. *J. Atmos. Sci.*, **40**, 215–229.

Liou, K. N., Ou, S. S., Kinne, S., Koenig, G., 1984: Radiation parameterization programs for general circulation models. Air Force Geophysics Laboratory, AFGL-TR-84-0217, 53 pp.

Liou, K. N., Sasamori, T., 1975: On the transfer of solar radiation in aerosol atmospheres. *J. Atmos. Sci.*, **32**, 2166–2177.

Liou, K. N., Wittman, G. D., 1979: Parameterization of the radiative properties of clouds. *J. Atmos. Sci.*, **36**, 1261–1273.

London, J., 1957: A study of the atmospheric heat balance. Final Report, Contract AF 19 (122)-165 (AFCRC-TR-57-287), New York University [ASTIN 117227], 99 pp.

Manabe, S., Möller, F., 1961: On the radiative equilibrium and heat balance of the atmosphere. *Mon. Wea. Rev.*, **89**, 503–552.

McClatchey, R. A., Fenn, R. W., Selby, J. E. A., Voltz, F. E., Garing, J. S., 1971: Optical properties of the atmosphere. AFCRL Environmental Research Papers, No. 354, 85 pp.

Oort, A. H., 1983: *Global Atmospheric Circulation Statistics, 1958–1973*. NOAA Prof. Paper 14, U.S. Dept. of Commerce, 180 pp.

Oort, A. H., Péixoto, J. P., 1983: Global angular momentum and energy balance requirements from observations. *Adv. Geophys.*, **25**, *Theory of Climate*, New York: Academic Press, 355–505.

Oort, A. H., Rasmusson, E. M., 1971: *Atmospheric Circulation Statistics*. NOAA Prof. Paper 5, U.S. Dept. of Commerc, 323 pp.

Oort, A. H., Vonder Haar, T. H., 1976: On the observed annual cycle in the ocean-atmosphere heat balance over the Northern Hemisphere. *J. Phys. Oceanogr.*, **6**, 781–800.

Ou, S. S., Liou, K. N., 1983: Parameterization of carbon dioxide 15 μm band absorption and emission. *J. Geophys. Res.*, **88**, 5203–5207.

Ou, S. S., Liou, K. N., 1984: A two-dimensional radiative-turbulent climate model. I: Sensitivity to cirrus radiative properties. *J. Atmos. Sci.*, **41**, 2289–2309.

Robock, A., 1980: The seasonal cycle of snow cover, sea ice, and surface albedo. *Mon. Wea. Rev.*, **108**, 267–285.

Sasamori, T., London, J., Hoyt, D. V., 1972: Radiation budget of the Southern Hemisphere. In: *Meteorology of the Southern Hemisphere, Meteor. Mongr.*, **13**, 263 pp.

Sellers, W. D., 1965: *Physical Climatology*. University of Chicago Press, 272 pp.

Stephens, G. L., Campbell, G. C., Vonder Haar, T. H., 1981: Earth radiation budgets. *J. Geophys. Res.*, **86**, 9739–9760.

Vonder Haar, T. H., Suomi, V. E., 1971: Measurements of the earth's radiation budget from satellites during a five-year period. Part I: Extended time and space means. *J. Atmos. Sci.*, **38**, 305–314.

Authors' address: Szu-cheng S. Ou, K. N. Liou, and W. J. Liou, Department of Meteorology, University of Utah, Salt Lake City, UT 84112, U.S.A.

Printed in Austria